Progress In Electromagnetics Research, Vol. 156, 47–53, 2016

Design and Measurement of Multi-Frequency Antennas for RF Energy Harvesting Tags

Céline Leclerc[1, 2, *], Matthieu Egels[1, 2], and Emmanuel Bergeret[1, 2]

Abstract—In this paper, a methodology to design non-50 Ω antennas for energy harvesting is presented. Two prototypes are simulated and realized on an epoxy substrate: one operating at 433 MHz and 900 MHz, the other at 900 MHz and 2.4 GHz. These antennas are designed to match the input impedances of an integrated radio-frequency harvester for an output voltage of 1 V, value chosen considering the voltage needed to power the new generation of micro-controllers and electronic circuits for the Internet of Things. The measurement results indicate a reflection coefficient below −10 dB at the frequencies of interest, validating the methodology.

1. INTRODUCTION

Nowadays, energy harvesting is a key point in a lot of systems. Typical example is the node of the Internet of Things (IoT) which must be energetically autonomous. To achieve this objective, it has to harvest energy in its surrounding and store it in batteries to supply devices. If photovoltaic energy is often presented to be a solution for harvesting (from the sun or from a lamp for instance), RF (radio-frequency) energy that can come from WiFi, home automation, or telecommunication can reach area without light. Complex systems are used to harvest these forms of energies, to convert them into a DC (Direct Current) voltage and eventually to store them. Most of the time, in case of RF energy it works for only one frequency. Besides, before the voltage converter, an antenna is used, operating at the selected frequency. This one must be matched to the harvesting chip.

In this paper, antennas for harvesting RF energy are presented. These kinds of antennas are often designed with a 50 Ω input impedance. Therefore matching networks are used to convert the antenna input impedance to the conjugate of the impedance of the chip Z^*_{chip} [1–4]. However, in case of energy harvesting, this solution is not suitable as it increases bulkiness and losses. At very low levels of harvesting, it is not possible to assume these losses. Thus a system with direct connexion and impedance matching must be used.

Moreover, in order to collect as much energy as possible, the antenna and the complete system must operate in several frequency bands. However, if creating a single frequency antenna with a complex input impedance is a known problem, it is a key challenge to design multi-frequency antennas with different complex input impedances in order to increase the harvested RF energy. Besides, using only one antenna and one circuit saves place and avoid the need to multiply circuits and antennas working each at only one frequency [5–7].

In Section 2 the design of this kind of antenna will be presented introducing methodology of design. Two antennas are presented: one operating at 433 MHz (home automation) and at 900 MHz (telephony) and another one at 900 MHz and 2.4 GHz (WiFi). The latter one is sized to be able to contain in a credit card. Main simulation results are presented.

Received 18 December 2015, Accepted 13 March 2016, Scheduled 13 May 2016

* Corresponding author: Celine Leclerc (celine.leclerc@im2np.fr).

[1] IM2NP (Institut Matériaux Microélectronique Nanosciences de Provence) UMR CNRS 7334, Technopôle de Château Gombert, Bâtiment FERMI, 5 rue Enrico Fermi, 13453 Marseille Cedex 13, France. [2] AMU (Aix-Marseille University), Jardin du Pharo, 58 bd Charles Livon, 13284 Marseille Cedex 07, France.

In Section 3, these antennas are realized, using a laser etching machine, on FR4 epoxy substrate. A way to efficiently characterize these kind of non-50 Ω antennas is discussed and applied to the realized antennas. Finally the main measurement results are shown and compared to the simulation results.

2. DESIGN: METHODOLOGY AND SIMULATION RESULTS

The aim of this work is to design an energy harvesting antenna operating at two arbitrary frequencies. Two independent cases are considered, with different frequency bands and similar antenna design. One is working at 433 MHz and 900 MHz (see Fig. 1(a)), the other one at 900 MHz and 2.4 GHz (see Fig. 1(b)). The antennas are simulated with HFSS [8], a finite element method solver for electromagnetic structure from Ansys, on a FR4 epoxy substrate of height $h = 1.6\,\text{mm}$, $\tan(\delta) = 0.02$, $\varepsilon_r = 4.4$, and copper thickness $t = 35\,\mu\text{m}$.

The methodology of design is similar in both cases. The idea is to use slotted bow-tie antennas [9–11]. The slotted design helps improve the targeted impedances, which have a positive imaginary part, and the form of the radiation pattern. First, the antenna at the lower frequency is designed. It has a slotted bow-tie form, alimented in its center. As a first approximation, the overall size of the antenna is of $\lambda_g/2$, with $\lambda_g = \lambda_0/\sqrt{\varepsilon_r} = \frac{c_0}{f_0\sqrt{\varepsilon_r}}$, with $c_0 = 3 \cdot 10^8\,\text{m} \cdot \text{s}^{-1}$ and f_0 the operating frequency. This length is modified to approximately reach the expected values of real and imaginary parts of the desired input impedance. The angles are filleted to help obtain the wanted input impedance and improve the gain. The aperture is modified to reach a trade-off between the input impedance and the gain, with an average value of 45° to begin.

When the low frequency antenna works, the antenna for the upper frequency is inserted inside it. Again, its maximal size is around $\lambda_g/2$. However, it cannot be connected at its center like previously. Instead, it is fed by coupling effects with the large antenna (for the lower frequency). In order to have these coupling effects, this second antenna has to be close enough to the first antenna. Therefore, the distance between the two antennas is fixed, as for the width of the inside antenna and the distance from the center. If the high frequency antenna is too close from the center, and thus from the excitation of the output antenna, the gain at the higher frequency can be highly deteriorated. The same problem emerges if the two antennas are too close from each other. Once these facts are considered, the modification of the geometry is similar: the length of $\lambda_g/2$ is changed to approximately reach the input impedance. Next, the angles are filleted and the aperture is tuned to improve the gain without impeding the input impedance. The aperture for the small antenna being modified, the one for the large antenna is also modified in order to keep the sides of both antennas parallel. Finally, the low frequency antenna needs to be slightly adjusted due to the insertion of the other antenna which brings slight coupling effects. It is a trade-off to obtain the expected impedances without degrading the radiation patterns and the value of the gains.

The chip used with these antennas is a custom-made chip [12, 13] which has a measured input impedance at 433 MHz for an output voltage of 1 V which is around $425 - j1200$. For 900 MHz, it is

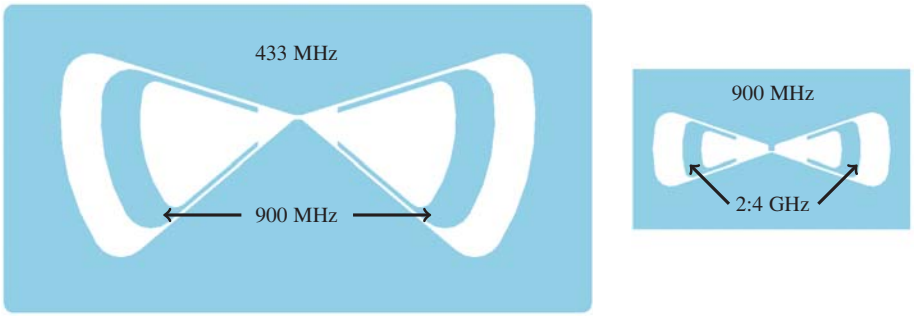

Figure 1. Antennas operating at two frequencies (the metallic portions are in grey). (a) 433 MHz and 900 MHz. (b) 900 MHz and 2.4 GHz.

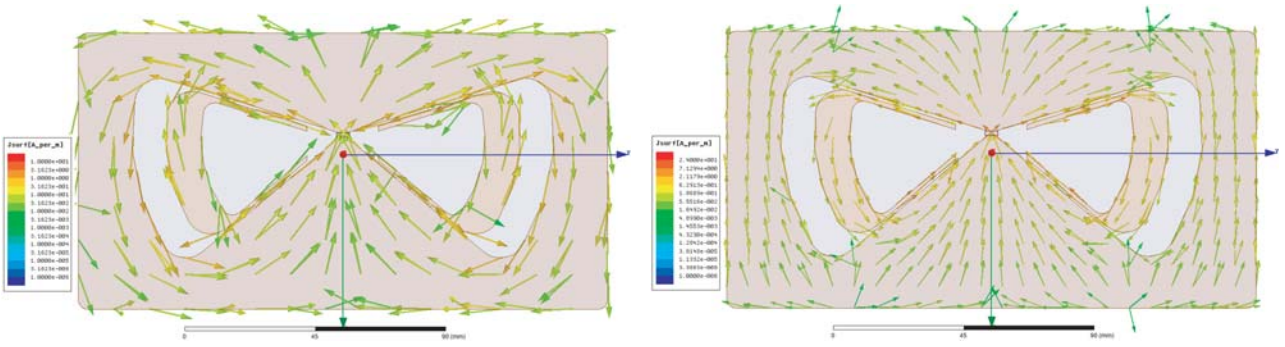

(a) (b)

Figure 2. Vector of the surface current distribution on the 433 MHz and 900 MHz antenna. (a) At 433 MHz (lower frequency). (b) At 900 MHz (higher frequency).

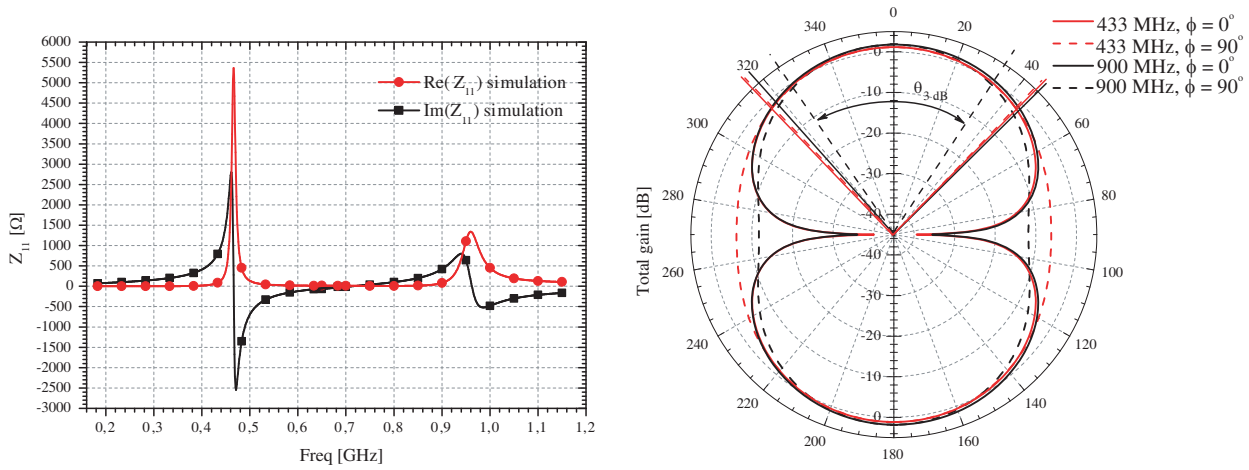

(a) (b)

Figure 3. Simulation results of the antenna operating at 433 MHz and 900 MHz. (a) Simulated impedances. (b) Simulated gain.

$85-j570$ and for 2.4 GHz, it is $14-j208$. The antennas are designed to be matched to these impedances, using the above mentioned procedure.

First the antenna operating at 433 MHz and 900 MHz is designed. Its global size is 18.5 cm × 9.5 cm. Simulating this antenna with a lumped port, Fig. 2 illustrates how the vectors of the surface current are distributed. It validates that at 433 MHz (Fig. 2(a)) the maximum of currents are on the outer antenna and that at 900 MHz (Fig. 2(b)) they are on the inner antenna. The impedances are displayed in Fig. 3(a). There is a little frequency shift compared as the expected value, placing the resonance (determined by Eq. (1)) respectively at 447 MHz with a return loss value of −11.7 dB and 913 MHz with $\Gamma = -10.1$ dB. As for the radiation, at 433 MHz, the total gain is of 1.1 dB and at 900 MHz, it is of 1.8 dB (see Fig. 3(b)).

$$\Gamma = \frac{Z_{chip} - Z_{11}^*}{Z_{chip} + Z_{11}} \tag{1}$$

The same design procedure is used to create an antenna working at 900 MHz and 2.4 GHz. As mentioned in the introduction, its size matches to a credit card format: 54 mm × 85.6 mm. The main results are presented in Fig. 4(a) and are summarized in Table 1. Again there is a frequency shift at both operating frequencies, with a return loss $\Gamma = -18.0$ dB at 887 MHz and $\Gamma = -10.1$ dB at 2.362 GHz. However, it can still be slightly improved by adjusting the geometric parameters of the antenna. As for the gain, it is of 1.9 dB at 900 MHz and −0.7 dB at 2.4 GHz (see Fig. 4(b)).

Table 1. Simulated impedances and gain maximal values at several frequencies.

Antenna	Frequency	433 MHz	900 MHz	2.4 GHz
	Z_{chip}	$425 - j1200$	$85 - j570$	$14 - j208$
433 MHz + 900 MHz	$Z_{antenna} = Z_{11}$	$87 + j795$	$81 + j423$	
	$\Gamma_{\min}$ (dB)	-11.7 dB @447 MHz	-10.1 dB @913 MHz	
	G_{tot} (dB)	1.1 dB	1.8 dB	
	$\theta_{3\,\mathrm{dB}}(^\circ)$, at $\phi = 0^\circ$	$\pm 44.4^\circ$	$-41.5^\circ/+45^\circ$	
900 MHz + 2.4 GHz	$Z_{antenna} = Z_{11}$		$98 + j674$	$31 + j248$
	$\Gamma_{\min}$ (dB)		-18.0 dB @887 MHz	-10.1 dB @2.362 GHz
	G_{tot} (dB)		1.9 dB	-0.7 dB
	$\theta_{3\,\mathrm{dB}}$ $(^\circ)$, at $\phi = 0^\circ$		$-44.0^\circ/+44.2^\circ$	$-38.7^\circ/+38.9^\circ$

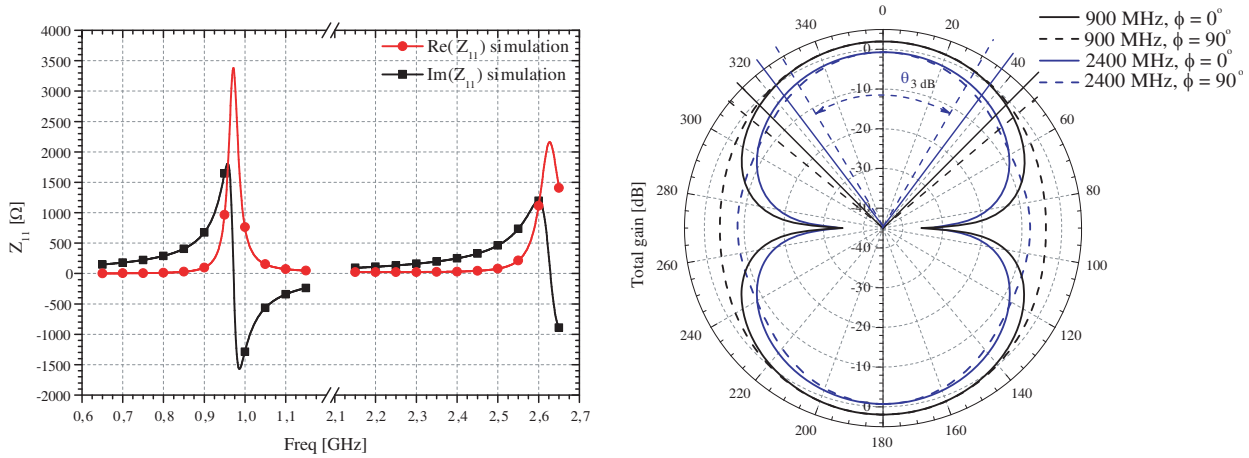

(a) (b)

Figure 4. Simulation results of the antenna operating at 900 MHz and 2.4 GHz. (a) Simulated impedances. (b) Simulated gain.

3. MEASUREMENT

These two antennas have been realized with a laser engraving machine on a FR4 substrate (see Fig. 5).

The first idea to measure the input impedance of these antennas is to solder a connector at the back of the board. However, it remains difficult to access to a proper measurement of the impedance, which has a strong positive imaginary part, placing the impedance at the right of the Smith chart.

Another way is to use a differential probe as presented in [14] (Fig. 6). It consists of two rigid copper coax of the same length. Their outer conductors are soldered together. The two inside conductors are used to convey the signals. With this kind of probe, the antenna is not connected to the ground (the outer conductor of the coax).

First, the VNA (Vector Network Analyser) is calibrated. Then the differential probe is added at the end of the calibration plan. The electrical delay on each port of the probe is determined. Next, the probe is soldered to the antenna through its back (to less disturb the radiation). The differential return loss is plotted on a Smith chart and the differential input impedance is observed at the frequencies

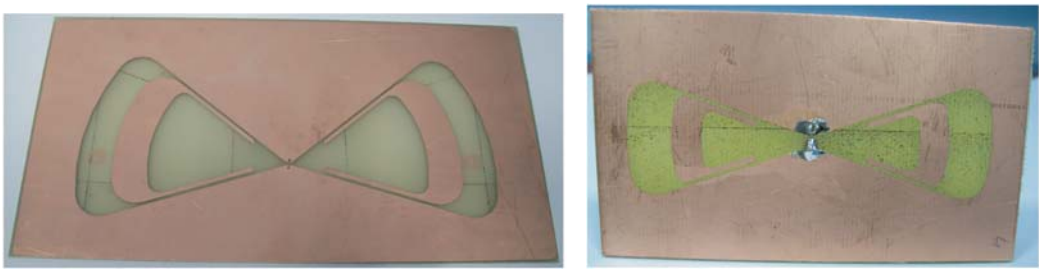

(a) (b)

Figure 5. Antennas operating at two frequencies. (a) 433 MHz and 900 MHz. (b) 900 MHz and 2.4 GHz.

Figure 6. Differential probe used to characterize the antennas.

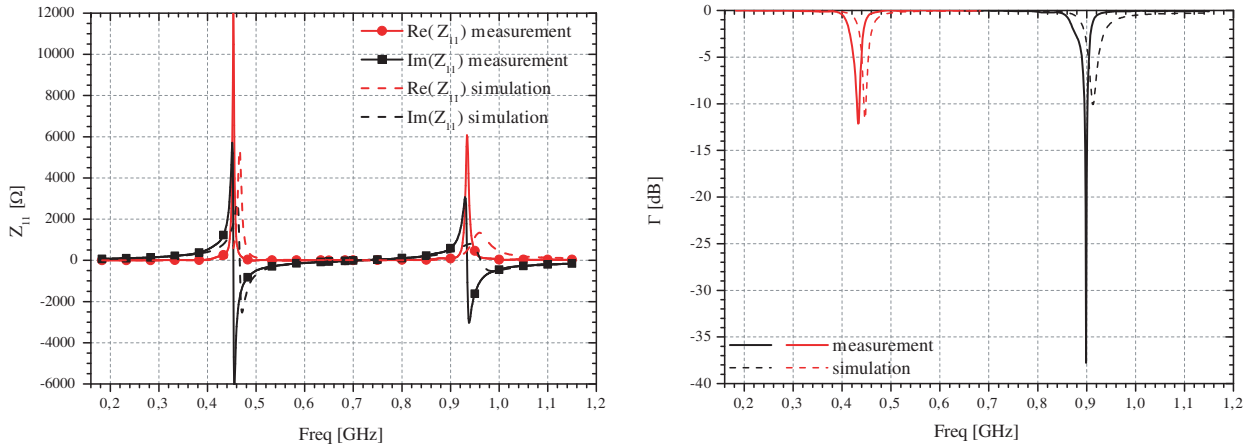

(a) (b)

Figure 7. Measurement results of the antenna operating at 433 MHz and 900 MHz. (a) Measured differential impedances compared to simulated impedances (dotted curves). (b) Measured refllection coefficient.

of interest. The used VNA (Anritsu MS4640B) automatically gives the differential input impedance. However, it can also be retrieved with the coefficients of the scattering matrix, using the formula given in Eq. (2). The electrical delay and the losses are adjusted on each port to match the expected impedance value at the frequencies of interest. The same is done at the two frequencies and for the two antennas.

$$Z_{ant}^{diff} = \frac{2Z_0\left(1 - S_{11}S_{22} + S_{12}S_{21} - S_{12} - S_{21}\right)}{\left(1 - S_{11}\right)\left(1 - S_{22}\right) - S_{12}S_{21}} \tag{2}$$

With this method, it appears that the simulated impedance and the measured differential impedance match (see Figs. 7 and 8) around the operating frequencies. Moreover, with this measurement technique, the return loss is below −10 dB at the frequencies of interest. It is a little better centred than it was in the simulation results. It appears that for both antennas the impedance value for 900 MHz is easier to obtain with a better reflection coefficient.

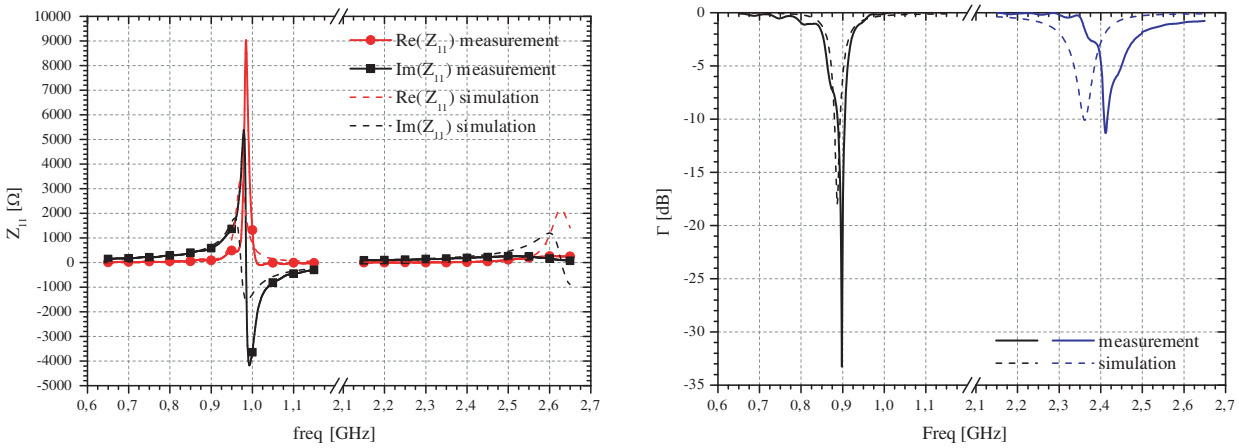

(a) (b)

Figure 8. Measurement results of the antenna operating at 900 MHz and 2.4 GHz. (a) Measured differential impedances compared to simulated impedances (dotted curves). (b) Measured reflection coefficient.

As for the gain of these antennas, it is determined using a known antenna (with a gain G_{Tx}) positioned at a distance $d = 2.5\,\mathrm{m}$. The antenna is still soldered to a differential probe. The VNA gives the magnitude of the differential reflection coefficient S_{DD} and the value of the transfer coefficient between the differential port of the measured antenna and the single port of the known antenna S_{DX}. Thus, with the Friis formula [9] given in Eq. (3), the gain can be retrieved.

$$G\,[\mathrm{dB}] = 10\log_{10}\left(1 - |S_{DD}|^2\right) - G_{Tx}\,[\mathrm{dB}] - 20\log_{10}\left(\frac{\lambda}{4\pi d}\right) - 20\log_{10}\left(|S_{DX}|\right) \tag{3}$$

The impedance being strongly complex, the antenna is matched only around the frequencies of interest. Thus the value of the measured gain is reliable only for these frequencies. Moreover there are multiple reflections in the cables that disturb the results. Despite these perturbations, around the center frequencies, the measured gain is close to the simulated gain with a value of 2.2 dB at 433 MHz (1.1 dB in simulation) and 1.7 dB at 900 MHz (1.8 dB in simulation) for the antenna from Fig. 5(a). For the antenna from Fig. 5(b), the measured gain reaches 1.5 dB at 900 MHz (1.9 dB in simulation) and −1.6 dB at 2.4 GHz (−0.7 dB in simulation). The main results are recapitulated in Table 2.

Table 2. Measured impedances and gain maximal values at several frequencies.

Antenna	Frequency	433 MHz	900 MHz	2.4 GHz
	Z_{chip}	$425 - j1200$	$85 - j570$	$14 - j208$
433 MHz + 900 MHz	$Z_{antenna} = Z_{11}$	$258 + j1229$	$87 + j591$	
	$\Gamma_{\min}$ (dB)	−12.1 dB @433 MHz	−37.8 dB @899 MHz	
	G_{tot} (dB)	2.2 dB	1.7 dB	
900 MHz + 2.4 GHz	$Z_{antenna} = Z_{11}$		$86 + j587$	$15 + j187$
	$\Gamma_{\min}$ (dB)		−33.3 dB @898 MHz	−11.3 dB @2.411 *GHz*
	G_{tot} (dB)		1.5 dB	−1.6 dB

4. CONCLUSION — FUTURE WORK

With this paper, a procedure to design non-50 Ω antennas operating at two distinct frequencies was presented. Moreover, an ingenuous technique has been used to measure impedance which was proved efficient, with a good concordance with the simulation results.

Future work will focus in better considering the variation of the chip impedance over frequency to improve the antenna bandwidth. It also includes assembling the integrated circuit and the antennas with bonding. Finally, the output voltage received by the complete device will be measured.

ACKNOWLEDGMENT

This work is supported by Apodise project.

REFERENCES

1. Dini, M., M. Filippi, A. Costanzo, A. Romani, M. Tartagni, M. Del Prete, and D. Masotti, "A fully-autonomous integrated RF energy harvesting system for wearable applications," *2013 European Microwave Conference (EuMC)*, 987–990, October 2013.
2. Pinuela, M., P. D. Mitcheson, and S. Lucyszyn, "Ambient RF energy harvesting in urban and semi-urban environments," *IEEE Transactions on Microwave Theory and Techniques*, Vol. 61, No. 7, 2715–2726, July 2013.
3. Li B., S. Xi, N. Shahshahan, N. Goldsman, T. Salter, and G. M. Metze, "An antenna co-design dual band RF energy harvester," *IEEE Transactions on Circuits and Systems I: Regular Papers*, Vol. 60, No. 12, 3256–3266, December 2013.
4. Niotaki, K., S. Kim, S. Jeong, A. Collado, A. Georgiadis, and M. Tentzeris, "A compact dual-band rectenna using slot-loaded dual band folded dipole antenna," *IEEE Antennas and Wireless Propagation Letters*, Vol. 12, 1634–1637, 2013.
5. Kuhn, V., C. Lahuec, F. Seguin, and C. Person, "A multi-band stacked RF energy harvester with RF-to-DC efficiency up to 84%," *IEEE Transactions on Microwave Theory and Techniques*, Vol. 63, No. 5, 1768–1778, May 2015.
6. Parks, A. N. and J. R. Smith, "Sifting through the airwaves: Efficient and scalable multiband RF harvesting," *Proc. of IEEE International Conference on RFID*, 7481, April 2014.
7. Parks, A. N. and J. R. Smith, "Active power summation for efficient multiband RF energy harvesting," *Proc. of International Microwave Symposium*, 2015.
8. HFSS by Ansys, http://ansys.com/en-GB/Products/Electronics/ANSYS-HFSS.
9. Balanis, C. A., *Antenna Theory: Analysis and Design*, 3rd Edition, Wiley-Interscience, Hoboken, New Jersey, 2005.
10. Brown, G. H. and O. M. Woodward, "Experimentally determined radiation characteristics of conical and triangular antennas," *RCA Review*, Vol. 13, No. 4, 425–452, December 1952.
11. Booker, H. G., "Slot aerials and their relation to complementary wire aerials (Babinet's principle)," *Journal of the Institution of Electrical Engineers — Part IIIA: Radiolocation*, Vol. 93, No. 4, 620–626, 1946.
12. Bergeret, E., J. Gaubert, P. Pannier, and P. Rizzo, "Power generation system for UHF passive RFID," *Electronics Letters*, Vol. 42, No. 25, 1452–1454, December 2006.
13. Rizzo, P., E. Bergeret, J. Gaubert, and P. Pannier, "Contactless integrated circuit with high-efficiency electrical power supply circuit," patent US7580694 B2, August 2009.
14. Qing, X., C. K. Goh, and Z. N. Chen, "Impedance characterization of RFID tag antennas and application in tag co-design," *IEEE Transactions on Microwave Theory and Techniques*, Vol. 57, No. 5, 1268–1274, May 2009.